Nanoscale

Accepted Manuscript

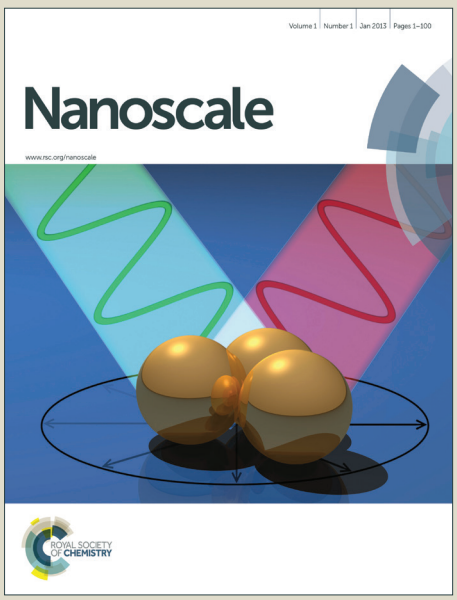

ROYAL SOCIETY OF CHEMISTRY

www.rsc.org/nanoscale

Oxidation and reduction processes of platinum nanoparticles observed at the atomic scale by environmental transmission electron microscopy

Hideto Yoshida,[a] Hiroki Omote,[ab] and Seiji Takeda*[a]

[a]*The Institute of Scientific and Industrial Research, Osaka University, 8-1 Mihogaoka, Ibaraki, Osaka 567-0047, Japan*
[b]*Division of Materials and Manufacturing Science, Graduate School of Engineering, Osaka University, 2-1 Yamadaoka, Suita, Osaka 565-0871, Japan*
**E-mail: takeda@sanken.osaka-u.ac.jp.*

Table of contents entry

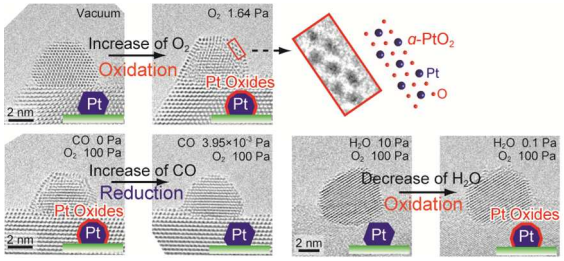

Atomic layers of Pt oxides were gradually formed on the surface of Pt nanoparticles in O_2 and the oxides were reduced to Pt promptly in both vacuum and gas including CO. H_2O vapor suppressed the surface oxidation.

Abstract

Oxidation and reduction of the surfaces of Pt nanoparticles were in situ examined in reactive gases (O_2, CO and H_2O vapor) by aberration-corrected environmental transmission electron microscopy. Atomic layers of Pt oxides were gradually formed on the surface of Pt nanoparticles

at room temperature in O_2. The surface Pt oxides were reduced to Pt promptly in both vacuum and gas including CO. We showed that H_2O vapor suppressed the surface oxidation. The processes found in this study were induced by gases that were most likely activated by electron irradiation. The observation results provide atomistic insights into the oxidation and reduction process of the surface of Pt nanoparticles that is exposed to activated gases.

1 Introduction

Oxidation and reduction are fundamental processes in catalytic reactions, corrosion, and organic synthesis. The surface of Pt nanoparticles has received special attention in the study of oxidation and reduction processes. Substantial experimental and theoretical investigations, for instance in the electrodes of fuel cells, have been made to correctly understand the processes in real space and time.[1–5] However, the formation and reduction processes of surface Pt oxides remain controversial at the atomic scale. Here we report in situ observation of the oxidation and reduction processes of the surface of Pt nanoparticles by atomic scale environmental transmission electron microscopy (ETEM). Pt oxides were formed gradually in O_2 and at room temperature and the oxides were reduced promptly to Pt by adding small amount of CO or H_2O vapor to the dominant O_2 gas. It is concluded that electron irradiation during ETEM observation activates the gases non-thermally, therefore promoting or suppressing the processes at room temperature. This study brought invaluable insight at the atomic scale into the states of the surface of Pt nanoparticles that is exposed to activated gases.

In catalytic chemistry, in situ observation methodologies such as electron microscopy, scanning probe microscopy, X-ray diffraction, X-ray photoelectron spectroscopy, and Raman spectroscopy have recently aroused broad interest.[6] When exploiting such in situ methodologies, it is indispensable to clarify the influence of measurement probes that are used on an object. Among in situ methodologies, ETEM allows atomic-scale observation of solid—gas and solid—liquid reactions.[7–13] ETEM has enhanced our understanding of the oxidation of Cu surfaces[14] and carbon nanotubes,[15] the reduction of Co_3O_4[16,17] and NiO particles,[18] and the oxidation and reduction of CeO_2 nanoparticles[19] and Pt-Co nanoparticles.[20] For further progress in this emerging in situ methodology, the influence of electron irradiation: heating of samples, ionization of gas and liquid, and knock-on of atoms in samples has to be carefully considered.[21–25] The present study clarified the effects of electron irradiation on the surface of Pt nanoparticles in different gases including H_2O vapor.

2 Experimental

Pt nanoparticles on CeO_2 supports (Pt/CeO_2) were prepared by solid grinding, which produced halogen-free supported metal nanoparticulate catalysts.[26,27] Details of the sample have been already described elsewhere.[27] The Pt/CeO_2 sample were supported on holly carbon films on Cu micro grids in air. A grid with the sample was set in a specimen holder with double tilt capability for ETEM observation. The ETEM (FEI Titan ETEM G2, equipped with a custom designed environmental cell (E-cell))[10] was equipped with a corrector for the spherical aberration of the objective lens. The operating voltage was 300 kV. The sample was studied at room temperature

under vacuum and also under O_2, CO/air (1 vol % CO, 21 vol % O_2, 78 vol % N_2), H_2O vapor, and mixtures of these gases. The residual gas pressure in vacuum in the ETEM was 1.0×10^{-5} Pa, and the partial pressures of the major constituent gases were 6.3×10^{-6}, 1.9×10^{-6} and 1.0×10^{-6} Pa for H_2O, O_2 and N_2, respectively, as measured by quadrupole mass spectrometry. It is noted that H_2O vapor is inevitably included as the dominant residual gas species in any conventional vacuum system. Before in situ ETEM observation in vacuum and gases, Pt nanoparticles were pre-inspected at lower magnification with a carefully controlled observation procedure (an electron current density, $\phi << 0.1$ A/cm^2 for centering an area of interest and focusing on the area in a viewing screen). To minimize electron-irradiation damage during in situ ETEM observation, images of the sample were recorded with an electron current density of 4.0 A/cm^2. Otherwise it is noted in text. The electron current density ($\phi = 4.0$ A/cm^2) is smaller than that in ordinary high resolution TEM observations; there were no detectable structural damages on Pt nanoparticles, CeO_2 supports or their interfaces during ETEM observation. The Pt nanoparticles were observed with an electron beam parallel to the [011] zone axis of crystalline fcc platinum, using the double tilt specimen holder. Images were recorded using a CCD camera, with a time resolution of 1.0 or 1.5 s per frame. The frame resolution was 1024 × 1024 pixels, with a bit depth of 16 bits. In the imaging condition, the atomic columns of heavy Pt appeared dark in both crystalline fcc platinum and platinum oxides with the incident electron beam being parallel to a proper zone axes. TEM image simulation was carried out using the MACTEMPAS software package (Total Resolutions, Berkeley, CA, USA), with the following parameters: an accelerating voltage of 300 kV, spherical aberration coefficient for the objective lens of 1 μm, chromatic aberration coefficient for the objective lens of 1.4 mm, objective aperture radius of 10 nm^{-1}, standard deviation for the mechanical vibration in the lateral plane of 0.05 nm, and defocus

of the objective lens of –16 nm. The degradation of ETEM images due to electron scattering by gases was not significant in the ranges of gas pressure in this study,[28] so it was not considered in the image simulation.

3 Results and discussion

The oxidation process of Pt nanoparticles at room temperature is summarized in Fig. 1. Before introducing O_2 into the E-cell, Pt nanoparticles had the bulk-truncated surface without any structural reconstruction (Fig. 1a): The distance between adjacent dark dots, or adjoining atom columns on the topmost surface layer, 0.241 ± 0.007 nm, corresponds well to that in the Pt {111} surface. O_2 was gradually introduced into the E-cell, as is indicated in Fig. 1j. When the O_2 pressure, $P(O_2)$ increased above about 0.8 Pa, the topmost surface layer of the Pt nanoparticle became partially unstable (Fig. 1c); the distance between adjoining atom columns on the (-11-1) facet increased significantly to 0.270 ± 0.008 nm. This newly formed surface structure was unstable in the range of O_2 pressure, 0.8 Pa < $P(O_2)$ < 1 Pa: This structure was formed and reverted to its original structure (pure platinum) repeatedly during ETEM observation (Fig. 1c and d). When $P(O_2)$ was over 1.3 Pa, the nanoparticle was entirely covered with the stable surface layer (Fig. 1e). After increasing O_2 pressure further, the change in structure gradually proceeded into inner lattice planes of the nanoparticle (Fig. 1f). When the electron current density is much lower (ϕ = 0.1 A/cm^2) than the ordinary one (ϕ = 4.0 A/cm^2), the surface of Pt nanoparticles remained unchanged even in O_2 of higher pressure ($P(O_2)$ = 10^2 Pa) and for prolonged observations (10 min).

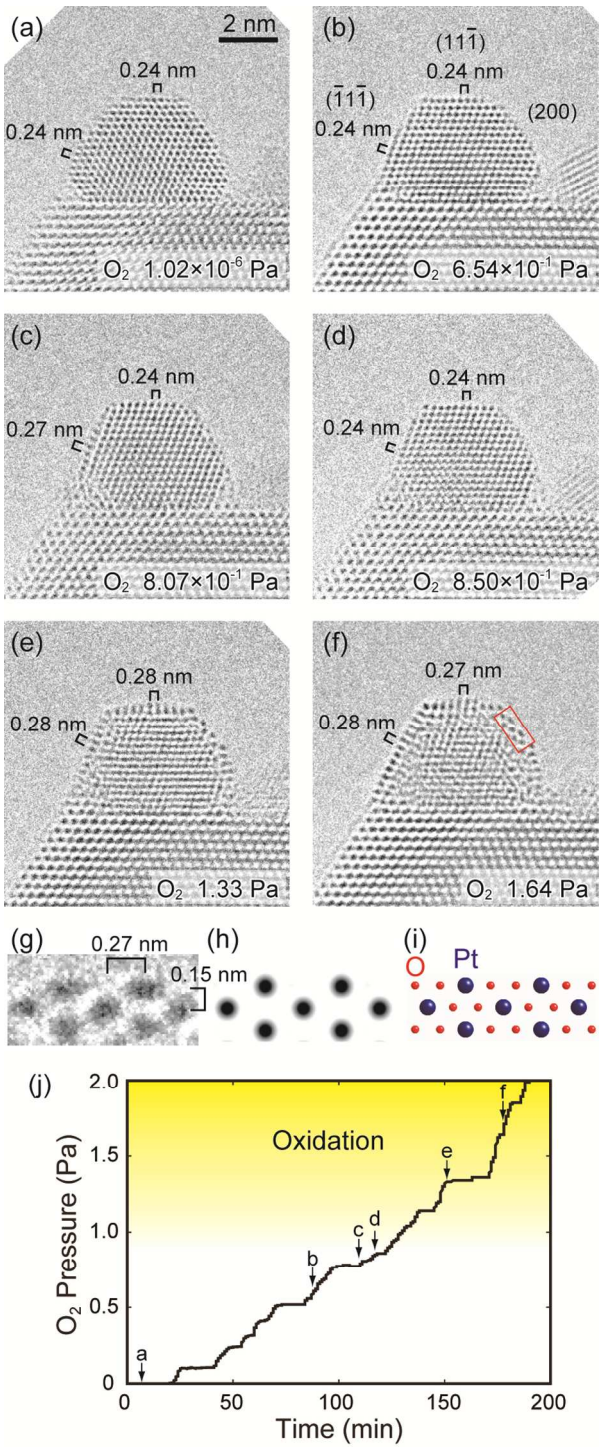

Fig. 1 Progress of oxidation at room temperature with increasing O_2 pressure. O_2 pressures were (a) 1.02×10^{-6} (residual O_2 in the vacuum), (b) 6.54×10^{-1} (c) 8.07×10^{-1} (d) 8.50×10^{-1} (e) 1.33 and (f) 1.64 Pa. A magnification of the surface of the Pt nanoparticle enclosed in (f) is shown in

(g). (h) Simulated image of an α-PtO_2 surface, based on the model shown in (i). (j) Increase in O_2 pressure with time measured by a built-in pressure gauge. The time and pressure of O_2 in recording the images in (a) to (f) are designated by a to f, respectively in (j). Electron current density, ϕ = 4.0 A/cm^2.

The stable surface layers were identified as previously known platinum oxides.[29-31] Figure 1g shows a representative magnified image of a surface structure with well-evolved oxidation. Given the well-defined arrangement of Pt atomic columns (Fig. 1g), image simulation was readily carried out for α-PtO_2 (hexagonal, a = 0.3113, c = 0.4342 nm)[29] with the principal [001] zone axis parallel to the viewing direction (Fig. 1h and i): The distances between the adjacent Pt atomic columns, 0.27 and 0.15 nm (Fig. 1g) agree well with those in α-PtO_2 (Fig. 1h and i). While the structure of this part could be determined (Fig. 1g-i), the other part did not exhibit well-defined image patterns owing to the misorientation of crystalline axes with regard to the electron beam. We estimated the spacing of the lattice fringes to be 0.27 to 0.28 nm (Fig. 1f). The spacing could not be accounted for by fcc platinum. Instead they may reflect the distances between adjoining Pt atom columns on the (001) plane of α-PtO_2 along the [100] zone axis (0.270 nm), (1-10) plane of β-PtO_2 (orthorhombic, a = 0.4488, b = 0.4533, c = 0.3138 nm)[30] along the [111] zone axis (0.282 nm), (010) plane of PtO (tetragonal, a = 0.305, c = 0.535 nm)[31] along the [100] zone axis (0.268 nm), and (1-10) plane of PtO along the [110] zone axis (0.268 nm). The surface of Pt nanoparticles was also in situ examined in O_2 ($P(O_2)$ = 100 Pa) by electron energy-loss spectroscopy (EELS). The O-K edge appeared at around 530 eV in EELS spectrum when an electron probe was placed on the surface area of a Pt nanoparticle (Fig. 2). Here, the background intensity resulting from O_2 gas was qualitatively subtracted from the EELS

spectrum. In addition, no Ce-M edges were found in the EELS spectrum (Fig. 2c), indicating that neither Ce oxides nor Pt-Ce-O existed on the surface of Pt nanoparticles. Based on the analysis of ETEM images combined with chemical analysis by EELS, it is concluded that the surface Pt oxides are formed stably in O_2 ($P(O_2)$ > 1.3 Pa) and at room temperature during ETEM observation.

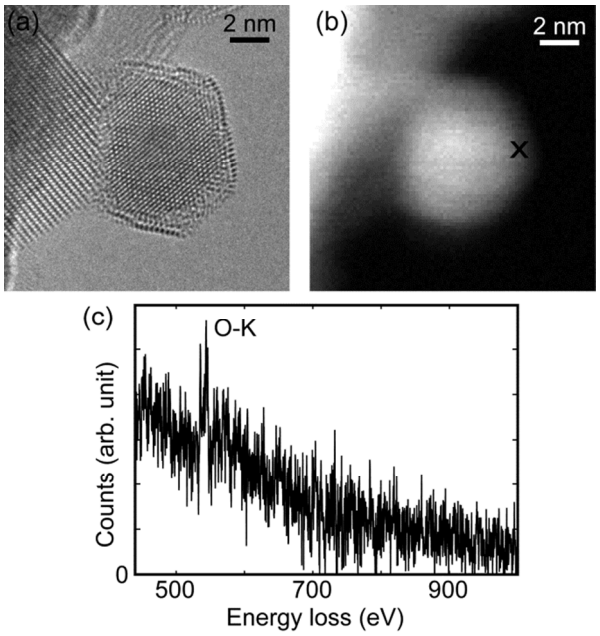

Fig. 2 Elemental analysis of a Pt nanoparticle in O_2 ($P(O_2)$ = 100 Pa) by EELS. (a) A TEM image and (b) a high-angle annular dark-field scanning transmission electron microscopy image of a Pt nanoparticle in O_2 ($P(O_2)$ = 100 Pa). (c) An EELS spectrum that was obtained from the point indicated in (b).

The surface Pt oxide can be reduced to Pt by adding CO to the dominant O_2 (Fig. 3). While being stable in thin CO (the partial pressure of CO, $P(CO) < 2.5\times10^{-3}$ Pa) (Fig. 3b), the surface Pt

oxide began to reduce partially in CO of higher partial pressure (P(CO) = 3×10^{-3} Pa), as is seen at the top right corner circled in Fig. 3c. With the further increase of the partial pressure of CO, Pt oxides on Pt (200) (Fig. 3d) and subsequently Pt (11-1) facets (Fig. 3e) were reduced. Finally, the surface Pt oxides were completely reduced to Pt at P(CO) = 4×10^{-3} Pa (Fig. 3f). After the reduction, the edges of the Pt nanoparticle became rounded, since {110}, {311} and other higher index facets appeared on the surface, as is shown in Fig. 3f. The rounded morphology of Pt nanoparticles under CO rich environments could be accounted for by the adsorption of CO on the surface of Pt nanoparticles.[27] Note that the partial pressure of CO was four to five orders of magnitude lower than that of O_2 when the surface Pt oxides was completely reduced.

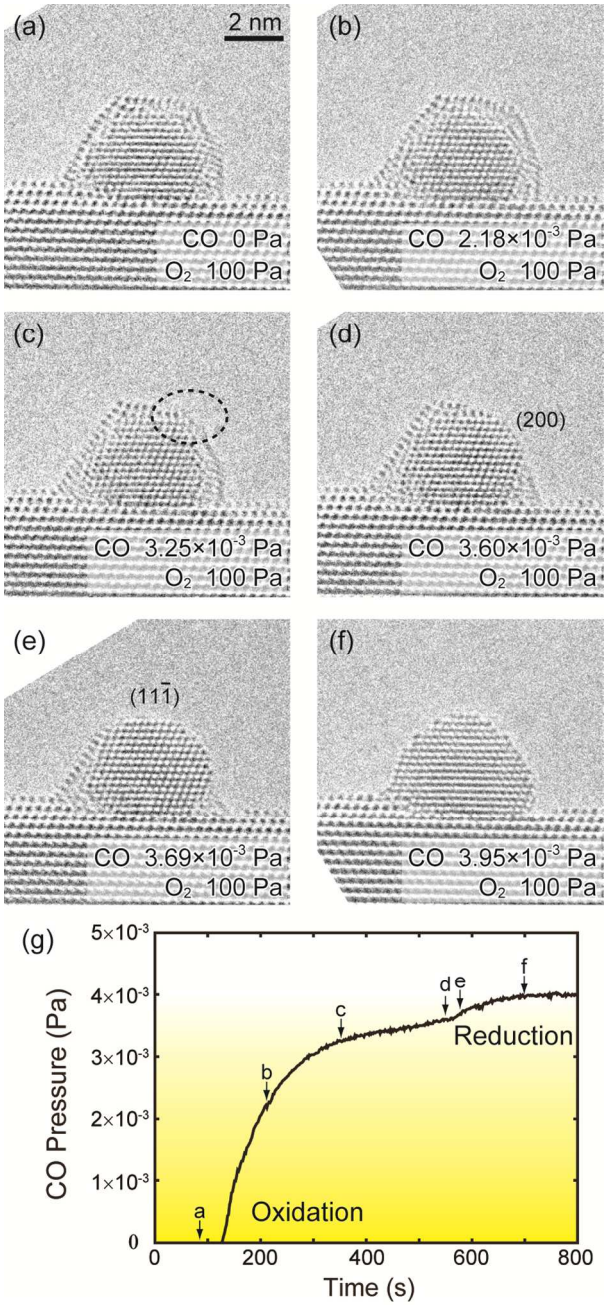

Fig. 3 Reduction process of an oxidized Pt nanoparticle by introducing CO. Partial pressure of CO, measured by quadrupole mass spectrometry was (a) 0, (b) 2.18×10^{-3}, (c) 3.25×10^{-3}, (d) 3.60×10^{-3}, (e) 3.69×10^{-3} and (f) 3.95×10^{-3} Pa. (g) The time and partial pressure of CO in recording the images in (a) to (f) are designated by a to f, respectively in (g). Partial pressure of

CO was increased by adding 1vol % CO/air to O_2 of 100 Pa. Electron current density, ϕ = 4.0 A/cm^2.

To clarify the effect of electron irradiation on the oxidation and reduction, we left Pt nanoparticles in the following gas flow experiments without electron irradiation except for final recording of ETEM images. The Pt nanoparticles were pre-inspected before the experiments as described above. After confirming that no oxide existed on the surface of Pt nanoparticle in vacuum (Fig. 4a), we interrupted ETEM observation and then introduced O_2 to the E-cell. The Pt nanoparticles were left in O_2 ($P(O_2)$ = 100 Pa) for 3 h without any electron irradiation. The surface of the Pt nanoparticles remained unchanged (no oxidation) (e.g. Fig. 4b). In another series of gas flow experiment, ETEM observation was interrupted, after the surface Pt oxide was fully formed in O_2 under electron irradiation (Fig. 5a). Subsequently, the E-cell was evacuated fully to vacuum. The Pt nanoparticle was observed with a carefully controlled observation procedure (ϕ = 0.1 A/cm^2 for centering an area of interest and focusing on the area in a viewing screen). Only 5 s after ϕ was increased to 4 A/cm^2, the surface Pt oxides remained only partially in an area indicated by arrow in Fig. 5b. The surface Pt oxides were completely reduced at 22 s (Fig. 5c). As a brief summary, electron irradiation was a necessary condition to create and annihilate surface Pt oxides.

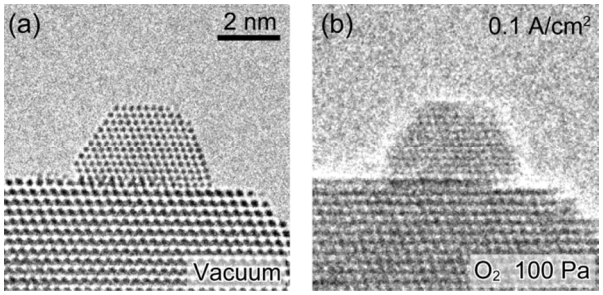

Fig. 4 Gas (O_2) flow experiment with minimal electron irradiation effect. A Pt nanoparticle (a) in vacuum at ϕ =4.0 A/cm^2 (as reference) and (b) in100 Pa O_2 at the low current density, ϕ = 0.1 A/cm^2. For detail, see text. (b) was acquired at an exposure time of 8 s due to the low current density. Upon increasing the electron current density from 0.1 A/cm^2 to 4 A/cm^2, the surface structure immediately changed to the Pt surface oxide (Not shown).

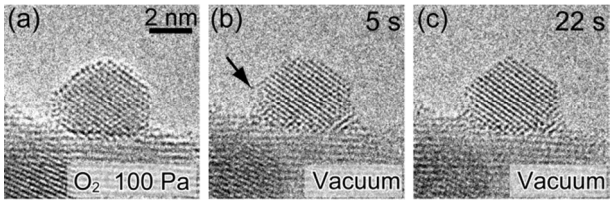

Fig. 5 Reduction of surface Pt oxide in vacuum by electron irradiation. (a) The initial oxidized Pt surface ($P(O_2)$ =100 Pa, ϕ =4.0 A/cm^2). ETEM observation was interrupted until full evacuation to vacuum. The surface Pt oxides were reduced (b) partially 5s and (c) fully 22s after ETEM observation (ϕ = 4.0 A/cm^2) was resumed.

It is well known that H_2O and OH molecules are adsorbed on Pt surfaces[32] in addition to apparent adsorbates (O_2 and CO). Since moisture is inevitably included in any environment unless a special care is made, we introduced H_2O vapor intentionally into the E-cell and

investigated the effect of H_2O vapor on the oxidation of Pt nanoparticles. To make the effect clear, we added H_2O vapor of different partial pressures to O_2 of constant partial pressure of 100 Pa, as is summarized in Fig. 6. It is noted that before introducing H_2O vapor into the E-cell, the partial pressure of residual H_2O vapor was low at $\sim 10^{-5}$ Pa. In a mixture of 10 Pa H_2O and O_2 (Fig. 6b), Pt nanoparticles were not oxidized even after prolonged ETEM observation for 20 min. After decreasing the partial pressure of H_2O ($P(H_2O)$) to 1 Pa, atomic layers of Pt oxide grew partially on the surface; the average distance between adjoining Pt atom columns was 0.28 nm on the (11-1) facet (Fig. 6c). In a mixture of H_2O of much lower partial pressure ($P(H_2O)$ = 0.1 Pa) and O_2, (-11-1) and (1-11) facets were oxidized and (11-1) and (200) facets were changed to be roughened (Fig. 6d). Oxidation did not proceed further into the inside of the Pt nanoparticle, even upon observing for 20 min in a mixture of H_2O ($P(H_2O)$ = 0.1 Pa) and O_2. Comparing the observation (Fig. 6) with Pt surfaces oxidized in O_2 with residual H_2O vapor (in the order of 10^{-5} Pa) (Fig. 1), one concludes that the oxidation is suppressed by H_2O vapor.

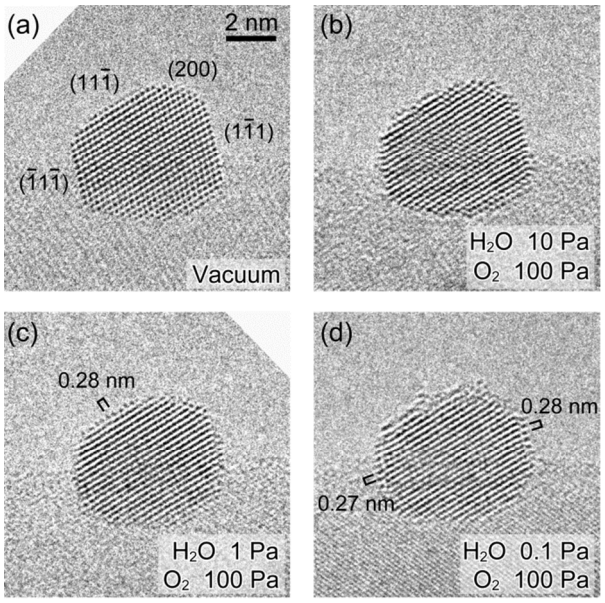

Fig. 6 Suppression of the oxidation of a Pt nanoparticle upon intentionally adding H_2O vapor to O_2 ($P(O_2)$ = 100 Pa). (a) In vacuum without oxidation (as reference), (b) in 10 Pa H_2O for complete suppression, (c) 1 Pa H_2O for partial suppression and (d) much less suppression in 0.1 Pa H_2O. Electron current density, ϕ = 4.0 A/cm^2.

We discuss briefly the mechanism of oxidation and reduction of Pt nanoparticles during ETEM observation. The oxidation and reduction processes depend on the partial pressures of O_2, CO and H_2O vapor and electron current density ϕ, as is illustrated in Fig. 7. Here, we qualitatively classified the different states of the surfaces during the oxidation and reduction processes according to the coverage of surface oxides that could be revealed by atomic-scale ETEM images (Fig. 1 to 6): I, Pure Pt surface; II, Partially oxidized surface; III, Fully oxidized surface; IV, Oxidation proceeds into the interior of nanoparticle. In this way, the observations shown in Fig. 1, 3, 4, 5, and 6 are summarized in Fig. 7 as black circles, red triangles, open circle, green circle, and blue squares, respectively. The partial pressures of gases in Fig. 7 are represented qualitatively, since the partial pressures of gases at the transition of surface coverage varied significantly depending on individual Pt nanoparticles. It is known that oxygen molecules are dissociatively adsorbed on a Pt surface at room temperature even in the absence of electron irradiation and that the maximum atomic oxygen coverage on Pt(111) is reportedly 0.25 monolayers.[33] This thermally equilibrium coverage is low and Pt oxides cannot form on the entire surface of Pt nanoparticles at room temperature. The formation of Pt oxides on the entire surface requires temperatures of 800–1000 °C in O_2.[34] During ETEM observations, the increase in temperature around Pt nanoparticles by electron irradiation was estimated to be less than 50 °C.[21] Therefore, the oxidation in ETEM was unlikely caused by heat. It is known that the

direct exposure to atomic oxygen leads to the oxidation of Pt nanoparticles at room temperature.[2] Oxygen molecules in gas phase likely decomposed upon electron irradiation, and the resulting atomic oxygen promotes the oxidation on the surface of Pt nanoparticle associated with the thermally dissociated oxygen even at room temperature. On the other hand, electron irradiation desorbs oxygen atoms from surface Pt oxides, thus reducing the surface Pt oxides (Fig. 5). The unstable surface oxide (Fig. 1c and d) is an evidence of the competing effects caused by electron irradiation. The balance of the competing effects depends on the partial pressure of gases and electron current density (Fig. 7). For instance, oxidation is promoted at higher partial pressure of O_2 ($P(O_2) > 1.3$ Pa) with a proper electron current density ($\phi \gg 0.1$ A/cm^2). CO and H_2O vapor act as effective reducing agents. Naturally, CO of even lower partial pressure ($P(CO) = 4 \times 10^{-3}$ Pa) reduced the surface Pt oxides at ϕ ranging from 0.1 to 4.0 A/cm^2. The reduction power of H_2O at room temperature (Fig. 6) should be attributed to electron irradiation. Under electron irradiation, H_2 molecules are produced from H_2O,[25] reducing surface Pt oxides. Therefore, the observation results could be accounted for by the non-thermal activation of various gases by electron irradiation. It is noteworthy that the oxidation started on the preferential facets of Pt nanoparticles by direct exposure to atomic oxygen (Fig. 1). Therefore, this study brought invaluable insight into the atomic processes on the surface of Pt nanoparticles that is exposed to activated gases. This study also calls attention to the effect of an electron probe that potentially biases atomic phenomena on a typically active surface of Pt interacting with reactive gases.

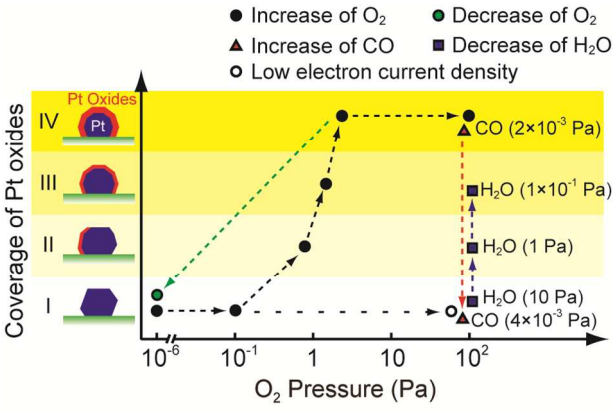

Fig. 7 Oxidation and reduction on the surface of Pt nanoparticles supported on CeO_2 during ETEM observation depending on O_2, CO and H_2O partial pressures, and the electron current density, ϕ. Black circles indicate the oxidation with increasing O_2 pressure. Green circles indicate the reduction with decreasing O_2 partial pressure. Red triangles indicate the reduction with increasing CO partial pressure. Blue squares indicate the suppression of oxidation by H_2O. ϕ = 4.0 A/cm^2 under all conditions, except for the condition marked by open circles (ϕ = 0.1 A/cm^2).

4 Conclusions

In conclusion, Pt nanoparticles supported on CeO_2 were oxidized in O_2 during ETEM observation at room temperature. In situ atomic resolution ETEM, combined with in situ EELS, showed that atomic layers of Pt oxides, including α-PtO_2 and Pt oxides of other forms, first started forming on the preferential facets of Pt nanoparticles at the early stage; entire oxidization on the whole surface of Pt nanoparticles then followed. The surface Pt oxides were promptly reduced to Pt in vacuum or by adding small amount of CO or H_2O vapor to dominant O_2. The effect of H_2O vapor on the processes was revealed in a systematic manner.

Acknowledgements

This study was partly supported by JSPS Grant-in-Aid for Scientific Research (A) Grant Number 25246003 and a Grant-in-Aid for Specially Promoted Research (No. 19001005), from the Ministry of Education, Culture, Sports, Science and Technology, Japan. The authors thank Prof. M. Haruta of the Tokyo Metropolitan University for supplying Pt/CeO_2 catalysts.

Notes and references

1 M. D. Ackermann, T. M. Pedersen, B. L. M. Hendriksen, O. Robach, S. C. Bobaru, I. Popa, C. Quiros, H. Kim, B. Hammer, S. Ferrer and J. W. M. Frenken, *Phys. Rev. Lett.*, 2005, **95**, 255505.

2 L. K. Ono, J. R. Croy, H. Heinrich and B. R. Cuenya, *J. Phys. Chem. C*, 2011, **115**, 16856−16866.

3 N. Seriani, Z. Jin, W. Pompe, L. C. Ciacchi, *Phys. Rev. B*, 2007, **76**, 155421.

4 H. Imai, K. Izumi, M. Matsumoto, Y. Kubo, K. Kato and Y. Imai, *J. Am. Chem. Soc.*, 2009, **131**, 6293−6300.

5 D. Friebel, D. J. Miller, C. P. O'Grady, T. Anniyev, J. Bargar, U. Bergmann, H. Ogasawara, K. T. Wikfeldt, L. G. M. Pettersson and A. Nilsson, *Phys. Chem. Chem. Phys.*, 2011, **13**, 262−266.

6 I. L. C. Buurmans and B. M. Weckhuysen, *Nature Chem.*, 2012, **4**, 873-886.

7 P. L. Gai, E. D. Boyes, S. Helveg, P. L. Hansen, S. Giorgio and C. R. Henry, *MRS Bulletin*, 2007, **32**, 1044−1050.

8 H. Yoshida, S. Takeda, T. Uchiyama, H. Kohno and Y. Homma, *Nano Lett.*, 2008, **8**, 2082−2086.

9 J. M. Yuk, J. Park, P. Ercius, K. Kim, D. J. Hellebusch, M. F. Crommie, J. Y. Lee, A. Zettl and A. P. Alivisatos, *Science*, 2012, **336**, 61−64.

10 S. Takeda and H. Yoshida, *Microscopy*, 2013, **62**, 193−203.

11 A. T. DeLaRiva, T. W. Hansen, S. R. Challa and A. K. Datye, *J. Catal.*, 2013, **308**, 291−305.

12 H. Yoshida and S. Takeda, *Carbon*, 2014, **70**, 266−272.

13 J. R. Jinschek, *Chem. Commun.*, 2014, **50**, 2696−2706.

14 G. Zhou, L. Luo, L. Li, J. Ciston, E. A. Stach and J. C. Yang, *Phys. Rev. Lett.*, 2012, **109**, 235502.

15 A. L. Koh, E. Gidcumb, O. Zhou and R. Sinclair, *ACS Nano*, 2013, **7**, 2566−2572.

16 S. Zhang, J. Shan, Y. Zhu, L. Nguyen, W. Huang, H. Yoshida, S. Takeda and F. F. Tao, *Nano Lett.*, 2013, **13**, 3310−3314.

17 M. R. Ward, E. D. Boyes and P. L. Gai, *Chem. Cat. Chem.*, 2013, **5**, 2655−2661.

18 Q. Jeangros, T. W. Hansen, J. B. Wagner, C. D. Damsgaard, R. E. Dunin-Borkowski, C. Hébert, J. Van herle and A. Hessler-Wyser, *J. Mater. Sci.*, 2013, **48**, 2893−2907.

19 R. Wang, P. A. Crozier and R. Sharma, *J. Phys. Chem. C*, 2009, **113**, 5700−5704.

20 H. L. Xin, S. Alayoglu, R. Tao, A. Genc, C.-M. Wang, L. Kovarik, E. A. Stach, L.-W. Wang, M. Salmeron, G. A. Somorjai and H. Zheng, *Nano Lett.*, 2014, **14**, 3203−3207.

21 T. Uchiyama, H. Yoshida, Y. Kuwauchi, S. Ichikawa, S. Shimada, M. Haruta and S. Takeda, *Angew. Chem. Int. Ed.*, 2011, **50**, 10157−10160.

22 H. Yoshida, Y. Kuwauchi, J. R. Jinschek, K. Sun, S. Tanaka, M. Kohyama, S. Shimada, M. Haruta and S. Takeda, *Science*, 2012, **335**, 317−319.

23 Y. Kuwauchi, H. Yoshida, T. Akita, M. Haruta and S. Takeda, *Angew. Chem. Int. Ed.*, 2012, **51**, 7729−7733.

24 Y. Kuwauchi, S. Takeda, H. Yoshida, K. Sun, M. Haruta and H. Kohno, *Nano Lett.*, 2013, **13**, 3073−3077.

25 J. M. Grogan, N. M. Schneider, F. M. Ross and H. H. Bau, *Nano Lett.*, 2014, **14**, 359−364.

26 S. Shimada, T. Takei, T. Akita, S. Takeda and M. Haruta, *Stud. Surf. Sci. Catal.*, 2010, **175**, 843−846.

27 H. Yoshida, K. Matsuura, Y. Kuwauchi, H. Kohno, S. Shimada, M. Haruta and S.Takeda, *Appl. Phys. Express*, 2011, **4**, 065001.

28 H. Yoshida and S. Takeda, *Phys. Rev. B*, 2005, **72**, 195428.

29 J. R. McBride, G. W. Graham, C. R. Peters and W. H. Weber, *J. Appl. Phys.*, 1991, **69**, 1596−1604.

30 S. Siegel, H. R. Hoekstra and B. S. Tani, *J. Inorg. Nucl. Chem.*, 1969, **31**, 3803−3807.

31 P. Villars and L. D. Calvert, *Pearson's handbook of crystallographic data for intermetallic phases*: American Society for Metals, 1985.

32 H. S. Casalongue, S. Kaya, V. Viswanathan, D. J. Miller, D. Friebel, H. A. Hansen, J. K. Nørskov, A. Nilsson and H. Ogasawara, *Nat. Commun.*, 2013, **4**, 2817.

33 K. Mortensen, C. Klink, F. Jensen, F. Besenbacher and I. Stensgaard, *Surf. Sci.*, 1989, **220**, L701−L708.

34 M. Salmeron, L. Brewer and G. A. Somorjai, *Surf. Sci.*, 1981, **112**, 207−228.